Mask inspection microscopy with 13.2 nm table-top laser illumination

Fernando Brizuela,[1,*] Yong Wang,[1] Courtney A. Brewer,[1] Francesco Pedaci,[1] Weilun Chao,[2] Erik H. Anderson,[2] Yanwei Liu,[2] Kenneth A. Goldberg,[2] Patrick Naulleau,[2] Przemyslaw Wachulak,[1] Mario C. Marconi,[1] David T. Attwood,[2] Jorge J. Rocca,[1] and Carmen S. Menoni[1]

NSF ERC for Extreme Ultraviolet Science and Technology

[1]Colorado State University, Fort Collins, Colorado 80523, USA

[2]Center for X-ray Optics, Lawrence Berkeley National Laboratory, Berkeley, California 94720, USA

[*]Corresponding author: brizuela@engr.colostate.edu

Abstract

We report the demonstration of a reflection microscope that operates at 13.2-nm wavelength with a spatial resolution of 55±3 nm. The microscope uses illumination from a table-top EUV laser to acquire aerial images of photolithography masks with a 20 second exposure time. The modulation transfer function of the optical system was characterized.

OCIS codes: 110.7440, 140.7240, 180.7460

Extreme Ultraviolet Lithography (EUVL) is the leading technology for integrated circuit fabrication at the 22 nm half-pitch node, and a contender technology for the 32 nm node [1]. The successful implementation of this approach relies on the availability of EUVL masks free of printable defects. Therefore, there are pressing demands for the development of metrology tools capable of finding and characterizing printable amplitude and phase defects on the mask. The masks' resonant-reflective multilayer coatings and wavelength-specific response dictate the necessity of EUV-wavelength inspection.

Several techniques can be employed to detect and characterize mask defects. Scanning methods, based on deep ultraviolet (DUV) light, are highly efficient for detecting defects in a relatively short time, but are incapable of assessing their EUV-wavelength-specific morphology [2-4]. Instead, for defect characterization, full-field microscopes that operate at wavelengths around 13.5 nm, within the bandwidth Mo/Si multilayer coatings, and that can render high-resolution aerial images of the mask surface can be used. These actinic inspection tools, when designed to mimic the imaging characteristics of production EUVL steppers, produce a magnified copy of the aerial image that allows the evaluation of pattern and defect printability, independent of the response of the photoresist. Furthermore, these microscopes can be useful in defect repair evaluation for EUVL masks [3]. Demonstrations of actinic aerial microscopes have until now been conducted at synchrotron facilities where radiation from bending magnets provides the required illumination [5, 6]. Synchrotron-based actinic microscopes are capable of imaging amplitude and phase defects with a spatial resolution better than 100 nm [7].

Transitioning EUV inspection microscopes into compact devices that can be used to inspect EUVL masks on-site requires compact light sources that provide sufficient flux near 13.5 nm wavelength to acquire aerial images with short exposure times. Low resolution imaging

systems capable of locating defects but not resolve their morphology have been demonstrated using compact EUV incoherent sources [8, 9]. Due to their high brightness, table-top EUV lasers are attractive illumination sources for compact high-resolution microscopy [10, 11]. A 13.2-nm-wavelength table-top microscope capable of rendering images of transmissive samples with a spatial resolution better than 38 nm has been demonstrated [12]. However, the more challenging realization of a table-top reflection-mode microscope at this wavelength has not yet been realized. In this letter we report what to our knowledge is the first demonstration of an actinic table-top EUV reflection microscope that captures images with a half-pitch spatial resolution of approximately 55 nm, comparable to that obtained with synchrotron sources.

The microscope uses as its illumination source a table-top, plasma-based, collisional EUV laser that operates at a wavelength of 13.2 nm [13, 14]. This source is well suited for actinic mask inspection because Mo/Si multilayers have a reflectivity of about 55% at this wavelength. The laser beam is created by the amplification of spontaneous emission in a transient population inversion produced by electron impact excitation in a transition of nickel-like Cd ions. To generate the EUV laser pulses a plasma is created by heating a 4-mm-wide Cd slab target with a sequence of pulses from a chirped-pulse-amplification Ti:Sapphire laser system. Pre-pulses are focused into a 30-μm-wide × 4-mm-long line, which creates a plasma that is allowed to expand to reduce electron density gradients [13, 14]. A transient population inversion is subsequently achieved by rapidly heating the plasma with an intense ($\sim 1\times10^{14}$ W cm^{-2}), 6.7-ps-duration pulse impinging at a grazing incidence angle of 23 degrees. The laser is operated at 5 Hz repetition rate, producing a highly monochromatic ($\Delta\lambda/\lambda < 1\text{x}10^{-4}$) beam with a moderate spatial coherence (1/20 of the beam diameter) and an average power of approximately 1 μW [15].

The reflection microscope, housed in a 70×45×40 cm^3 vacuum chamber, is illustrated schematically in Fig. 1.a. The laser beam is directed by a 42°-incidence Mo/Si-coated flat mirror onto a condenser zone plate that focuses the light onto the sample. The reflected light is projected by an off-axis zone plate objective, forming an image on an EUV-sensitive back-illuminated CCD detector.

The condenser and objective zone plates were fabricated by electron beam lithography on a 40-nm-thick Ni layer deposited onto 100-nm-thick Si_3N_4 membranes [16]. The 5-mm-diameter condenser zone plate has an outer zone width of 100 nm, and at 13.2-nm wavelength, it has a 38 mm focal length, with a numerical aperture (NA_c) of 0.066. The condenser is slightly overfilled by the laser light and illuminates the EUV mask at a 6° angle of incidence from normal. This geometry mimics the mask illumination conditions of a 4×-demagnification EUVL stepper with a numerical aperture of 0.25 [15].

Figure 1.b shows a SEM micrograph of the objective zone plate. The objective zone plate is an off-axis sub-aperture of a full parent zone plate lens that would have a 330-µm diameter (dashed line in the figure), an outer zone width of 40 nm, and a focal length of 1 mm. The pupil diameter is 120 µm, defining a numerical aperture of 0.0625, and its center is displaced 100 µm from the axis of the parent zone plate, as shown. An uncoated rectangular aperture next to the off-axis objective zone plate, transmits the incoming condensed laser beam illumination. The beam passes through the 40-nm-thick Si_3N_4 support membrane twice, reducing the intensity by approximately 50%, The off-axis zone plate design enables near-normal incidence imaging of the mask surface, minimizes aberrations, and provides incoherent illumination conditions by matching the NA of the condenser [17].

In these experiments, the imaged object was the surface of a Mo/Si multilayer mirror with a patterned Ni absorber layer consisting of grating structures, with half-pitch sizes ranging from 80 to 500 nm. EUV images of four elbow patterns with 80, 100, 120 and 140 nm half-pitch are shown in Fig. 2, along with their respective intensity cross-sections (lineouts). The images were obtained using a 20 second exposure time, with the laser operating at a repetition rate of 5 Hz. The images have a field of view of approximately 5×5 μm^2. They were taken with a magnification of 610× at which each pixel on the CCD corresponds to 22 nm in the sample plane. As expected for a practically incoherent optical system, the images show no distinguishable coherence effects. Intensity cross-sections for each image were obtained by averaging five rows of pixels (almost 100 nm on the mask) across the horizontal and vertical grating lines.

The modulation transfer function (MTF) of the microscope was constructed using the intensity modulation data obtained from the images shown in Fig. 2. The modulation ($(M=I_{max}-I_{min})/I_{max}$) starts to roll off for structures smaller than 120 nm half-pitch, in agreement with simulations for a 0.0625 NA objective under incoherent illumination. At 80 nm half-pitch, the smallest grating pattern available on the sample, the measured intensity modulation is approximately 65%, a value significantly higher than the Rayleigh resolution value of 26.5%. This indicates that the spatial resolution of the microscope is below 80 nm.

In the absence of gratings structures with smaller lines, the characterization of the instrument's modulation transfer function was extended using a knife-edge test. For incoherent imaging conditions the 10% to 90% intensity transition across a sharp edge corresponds to twice the half-pitch grating resolution of the optical system [17]. Figure 4 shows the intensity cross-sections obtained across the image shown in the insert. The measurements yielded a 10% to

90% transition of 110±5 nm, corresponding to a half-pitch grating spatial resolution for the microscope of 55±3 nm.

The spatial resolution of the microscope was independently confirmed by analyzing the EUV images of Fig. 2 with the full-image correlation method described by Wachulak, et al. [18]. Using this correlation method, a half-pitch resolution of 53±10 nm was obtained. This resolution meets the specifications set for the 22 nm technology half-pitch node.

In summary, we have demonstrated an actinic table-top EUV reflection microscope with a partial coherence (σ) value of 1.0 and a spatial resolution of approximately 55 nm. To demonstrate that this technique can be used in EUVL actinic photomask inspection, images of absorber patterns on a Mo/Si multilayer mirror were obtained with 20 second exposure times.

We acknowledge the contribution of Dr. Georgiy Vaschenko and the support of the Engineering Research Centers Program of the National Science Foundation under NSF Award Number EEC-0310717.

This work was supported by the Director, Office of Science, Office of Basic Energy Sciences, of the U.S. Department of Energy under Contract No. DE-AC02-05CH11231

References

1. International Technology Roadmap for Semiconductors (http://www.itrs.net).
2. K. A. Goldberg, A. Barty, Y. Liu, P. A. Kearney, Y. Tezuka, T. Terasawa, J. S. Taylor, H.-S. Han, and O. R. I. Wood, "Actinic inspection of extreme ultraviolet programmed multilayer defects and cross-comparison measurements," Journal of Vacuum Science and Technology B **24**, 2824-28 (2006).
3. K. A. Goldberg, A. Barty, P. Seidel, K. Edinger, R. Fettig, P. A. Kearney, H.-S. Han, and O. R. I. Wood, "EUV and non-EUV inspection of reticle defect repair sites," in *Emerging Lithographic Technologies XI, SPIE Advanced Lighography*, (Proc. SPIE, 2007), 6517-6511.
4. K. A. Goldberg, S. B. Rekawa, C. D. Kemp, A. Barty, E. H. Anderson, P. A. Kearney, and H.-S. Han, "EUV mask reflectivity measurements with micron-scale spatial resolution," in *SPIE Advanced Lithography*, (Proc. SPIE, 2008), 6921-43.
5. K. A. Goldberg, in *SPIE 27th Annual BACUS Symposium on Photomask Technology*, 2007), 7630199.
6. H. Kinoshita, K. Hamamoto, N. Sakaya, M. Hosoya, and T. Watanabe, "Aerial Image Maks Inspection System for Extreme Ultraviolet Lithography," Japanese Journal of Applied Physics **46**, 6113-17 (2007).
7. K. A. Goldberg, Journal of Vacuum Science and Technology B **in press**(2008).
8. Y. Tezuka, M. Ito, T. Terasawa, and T. Tomie, "Actinic detection of multilayer defects on EUV mask blanks using LPP light source and dark-field imaging," in *Emerging Lighographic Technologies VIII*, (Proc. SPIE, 2004), 0277-0786X.

9. Y. Tezuka, T. Tanaka, T. Terasawa, and T. Tomie, "Sensitivity-limiting Factors of at-Wavelength Extreme Ultraviolet Lithography Mask Blank Inspection," Japanese Journal of Applied Physics **45**, 5359-72 (2006).

10. F. Brizuela, G. Vaschenko, C. Brewer, M. Grisham, C. S. Menoni, M. C. Marconi, J. J. Rocca, W. Chao, J. A. Liddle, E. H. Anderson, D. T. Attwood, A. V. Vinogradov, I. A. Artioukov, Y. P. Pershyn, and V. V. Kondratenko, "Reflection mode imaging with nanoscale resolution using a compact extreme ultraviolet laser," Optics Express **13**, 3983-88 (2005).

11. C. A. Brewer, F. Brizuela, P. Wachulak, D. H. Martz, W. Chao, E. H. Anderson, D. T. Attwood, A. V. Vinogradov, I. A. Artyukov, A. G. Ponomareko, V. V. Kondratenko, M. C. Marconi, J. J. Rocca, and C. S. Menoni, "Single-shot extreme ultraviolet laser imaging of nanostructures with wavelength resolution," Optics Letters **33**, 518-20 (2008).

12. G. Vaschenko, C. Brewer, E. Brizuela, Y. Wang, M. A. Larotonda, B. M. Luther, M. C. Marconi, J. J. Rocca, and C. S. Menoni, "Sub-38 nm resolution tabletop microscopy with 13 nm wavelength laser light," Optics Letters **31**, 1214-16 (2006).

13. J. J. Rocca, Y. Wang, M. A. Larotonda, B. M. Luther, M. Berrill, and D. Alessi, "Saturated 13.2 nm high-repetition-rate laser in nickellike cadmium," Optics Letters **30**, 2581-83 (2005).

14. Y. Wang, M. A. Larotonda, B. M. Luther, D. Alessi, M. Berrill, V. N. Shyaptsev, and J. J. Rocca, "Demonstration of high-repetition-rate tabletop soft-x-ray lasers with saturated output at wavelengths down to 13.9 nm and gain down to 10.9 nm," Physical Review A **72**(2005).

15. Y. Liu, Y. Wang, M. A. Larotonda, B. M. Luther, J. J. Rocca, and D. T. Attwood, "Spatial coherence measurements of a 13.2 transient nickel-like cadmium soft x-ray laser pumped at grazing incidence," Optics Express **14**, 12872-79 (2006).

16. E. H. Anderson, "Specialized Electron Beam Nanolithography for EUV and X-Ray Diffractive Optics," IEEE Journal of Quantum Electronics **42**, 27-35 (2006).

17. J. M. Heck, D. T. Attwood, W. Meyer-Ilse, and E. Anderson, "Resolution determination in X-ray microscopy: an analysis of the effects of partial coherence and illumination spectrum," Journal of X-Ray Science and Technology **8**, 95-104 (1998).

18. P. W. Wachulak, C. A. Brewer, F. Brizuela, C. S. Menoni, W. Chao, E. H. Anderson, R. A. Bartels, J. J. Rocca, and M. C. Marconi, "Analysis of extreme ultraviolet microscopy images of patterned nanostructures based on a correlation method," Journal of the Optical Society of America B **25**, B20-B26 (2008).

Figure captions

Fig. 1. a) Schematic illustration of the compact actinic reflection microscope (not to scale). b) Top: SEM image of the off-axis objective zone plate and uncoated window region. The dashed line indicates the extent of the 'parent' zone plate. Bottom: 40 nm half-pitch outer zones of the objective zone plate.

Fig. 2. Actinic images and intensity cross sections of elbow patterns with: a) 80 nm, b) 100 nm, c) 120 nm, and d) 140 nm. The images were obtained with an exposure time of 20 seconds and a magnification of ~610×. The lineouts show that all the periodic patterns are fully resolved.

Fig. 3. Microscope's modulation transfer function. The MTF was constructed using the line-outs from the images of Fig. 2 (open circles) and the knife-edge test (solid circle). The data points for the grating half-pitch are averages of intensity modulation values obtained for several cross-sections taken from the vertical and horizontal gratings.

Fig. 4. Knife-edge test for the EUV image shown in the insert. The 10% to 90% transition is 110±5 nm.

Figures

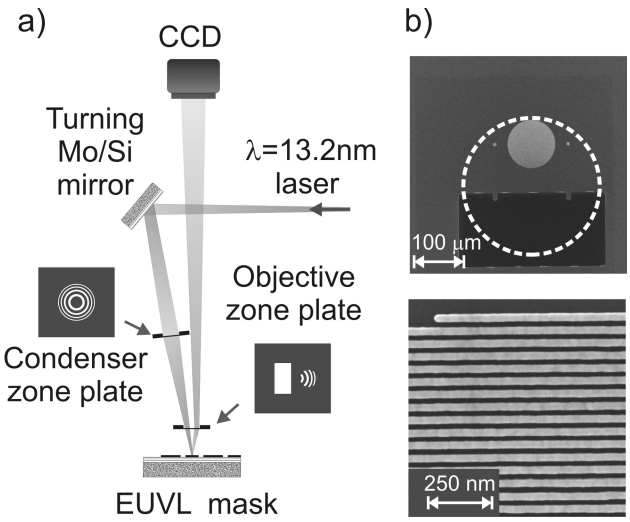

Fig.1

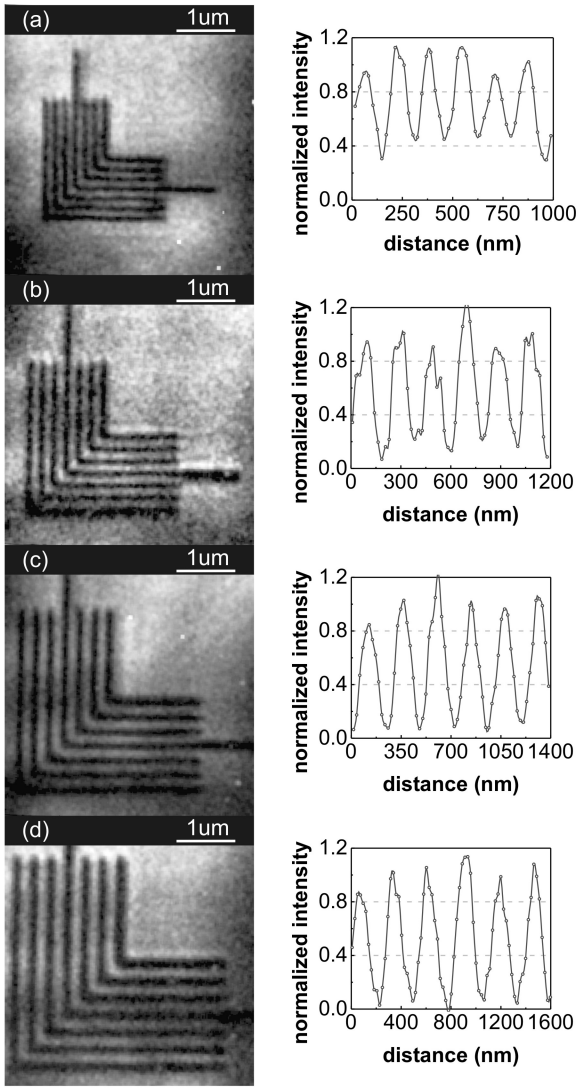
(a)
1um
(b)
1um
(c)
1um
(d)
1um
normalized intensity
1.2
0.8
0.4
0.0
0 250 500 750 1000
distance (nm)
normalized intensity
1.2
0.8
0.4
0.0
0 300 600 900 1200
distance (nm)
normalized intensity
1.2
0.8
0.4
0.0
0 350 700 1050 1400
distance (nm)
normalized intensity
1.2
0.8
0.4
0.0
0 400 800 1200 1600
distance (nm)

Fig. 2

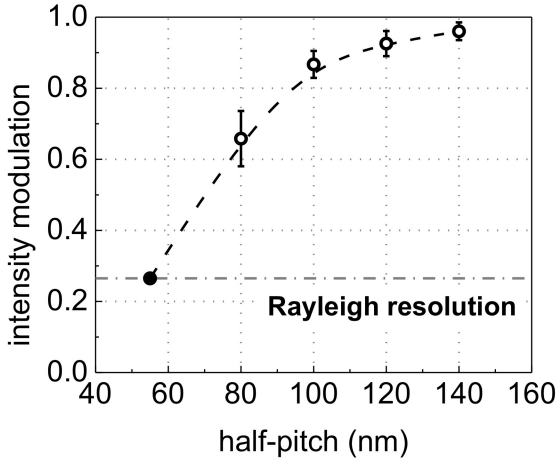
intensity modulation
half-pitch (nm)
Rayleigh resolution
1.0
0.8
0.6
0.4
0.2
0.0
40
60
80
100
120
140
160

Fig. 3

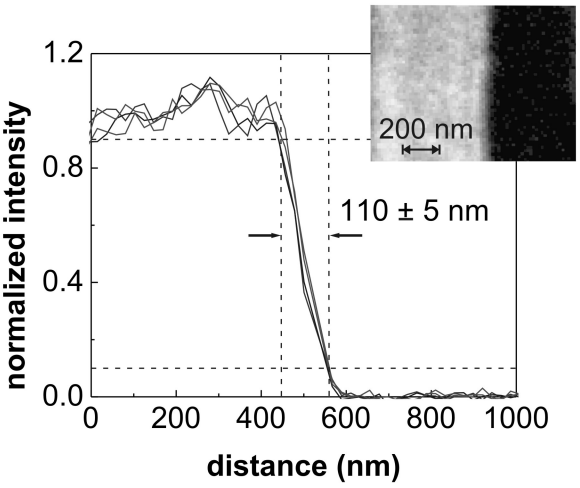
normalized intensity
distance (nm)
200 nm
110 ± 5 nm
1.2
0.8
0.4
0.0
0
200
400
600
800
1000

Fig. 4